International Journal of Automotive Technology, Vol. 17, No. 6, pp. 991−1002 (2016)
DOI 10.1007/s12239−016−0097−7

pISSN 1229−9138/ eISSN 1976−3832

ESTIMATION OF MAXIMUM ROAD FRICTION COEFFICIENT BASED ON LYAPUNOV METHOD

X. XIA[1, 2)], L. XIONG[1, 2)*], K. SUN[1, 2)] and Z. P. YU[1, 2)]

[1)]School of Automotive Studies, Tongji University, Shanghai 201804, China
[2)]National "2011" Collaborative Innovation Center, Tongji University, Shanghai 201804, China

(Received 2 March 2016; Revised 12 April 2016; Accepted 2 May 2016)

ABSTRACT−With the real time and accurate information of motor torque and rotation speed of the four-in-wheel-motor-drive electric vehicles, a slip based algorithm for estimating maximum road friction coefficient is designed using Lyapunov stability theory. Modified Burckhardt tire model is used to describe longitudinal slip property of the tire. By introducing a new state variable, a nonlinear estimator is proposed to estimate the longitudinal tire force and the maximum road friction coefficient simultaneously. With the appropriate selection of estimation gain, the convergence of the estimation error of the tire longitudinal force and maximum road friction coefficient is proved through Lyapunov stability analysis. In addition, the error is exponentially stable near the origin. Finally the method is validated with Carsim-Simulink co-simulation and real vehicle tests under multi working conditions in acceleration situation which demonstrate high computational efficiency and accuracy of this method.

KEY WORDS : Four-in-wheel-motor-drive electric vehicles, Estimation of maximum road friction coefficient, Lyapunov stability, Nonlinear estimator

1. INTRODUCTION

Vehicle dynamics control systems such as traction control system (TCS), anti-lock braking system/electric braking distribution system (ABS, EBD), electric stability control system (ESC) for improving vehicle active safety (Yu *et al.*, 2013) are realized by the forces at the interface between the tires and the road (Rajamani, 2005) which are strongly affected by the maximum road friction coefficient (Alvarez *et al*., 2004), therefore the accurate knowledge of the maximum road friction coefficient is significant for improving the vehicle active safety (Li *et al.*, 2013; Ahn *et al.*, 2012; Chen and Wang, 2011). It is difficult to estimate the maximum road friction coefficient for conventional vehicles with combustion engine or with single center motor because of the unknown torque and angular speed of the wheel. Based on the merits of the four-in-wheel-motor - drive electric vehicles that the motor torque and angular speed can be accurately known and quickly controllable (Hori, 2004), on the one hand it is more feasible to implement the vehicle dynamics control system on this kind of vehicles, on the other hand they have advantage to identify the maximum road friction coefficient than conventional vehicles (Yu *et al.*, 2006).

The state of the art for estimation of tire-road friction coefficient has been comprehensively illustrated in Müller *et al.* (2004) and Patel *et al.* (2008). Usually the road surface condition is included in the tire model implicitly (Li *et al.*, 2006), thus the modern commercial vehicles mostly estimate the maximum road friction coefficient through tire dynamics characteristics (tire model) including cornering characteristic (Ahn *et al.*, 2013; Haffner *et al.*, 2008) and longitudinal slip characteristic (Wit *et al.*, 2007; Gustafsson, 1997) instead of measuring it directly through sensors (Pohl *et al.*, 1999; Erdogan *et al.*, 2011; Sato *et al.*, 2007) with the consideration of cost. In order to increase the working range of the estimator and improve robustness, in Li *et al*. (2015), the longitudinal and lateral estimation results were merged based to give accurate maximum road friction coefficient under different maneuvers as far as possible. In Matuško *et al*. (2007), a neural-network-based method and an adaption law derived applying Lyapunov stability analysis were combined to estimate the road maximum friction coefficient. In Ray (1997), an extended Kalman filter (EKF) was used to estimate vehicle state and tire force through a high order vehicle model and then the maximum road friction coefficient was estimated based on longitudinal and lateral tire model with statistical methods using the information measured from standard sensors. In Qi *et al*. (2015) a novel tire model was proposed for the estimation of the tire-road interface characterization and based on this tire model an EKF was implemented to estimate the tire model parameters including the maximum road friction coefficient and slip slope. In Chen *et al*. (2015), the vehicle tire force was estimated by a KF (Kalman Filter) based on a high order vehicle model and

**Corresponding author.* e-mail: xiong_lu@tongji.edu.cn

then two UKF (Unscented KF) were adopted to obtain the maximum road friction coefficient in longitudinal and lateral direction respectively based on a modified Dugoff tire model. In Choi *et al*. (2013), the tire force was estimated in the same way, but the maximum road friction coefficient was identified through linearized recursive least squares methods with a forgetting factor based on a combined longitudinal and lateral brushed tire model. In Lin and Huang (2013), an UKF was adopted to estimate the tire longitudinal tire force and slip ratio in order to estimate the slip slope. Then the tire-road friction coefficient could be estimated by mapping the estimated slope to the friction values such as in Li *et al*. (2007) and Rajamani *et al*. (2010). However, some drawbacks still exist in those methods: 1) The convergence of estimation error could not be proved in those kind of KF method, and it is difficult to guarantee the convergence of estimation error, 2) Another disadvantage of using the KF method for road maximum friction estimation is that the computational load is large which means the real time validity is hard to guarantee (Imsland *et al*., 2006). Additionally, in an EKF, the nonlinear tire model must be linearized thus the accuracy is only first order due to the taylor linear approximation. The covariance matrix need to be adapted under different slip ratio and the stability of the estimator has to be considered more in those methods above. 3) Few experimental ground tests were conducted which are significant for validation of the effectiveness of those algorithm.

Compared with the kind of KF optimal estimation theory, nonlinear observers and methods based on logic rule can reduce the computational complexity in real time estimation. In Li *et al.* (2014), in rule-based method, according to the relationship between the nonlinearity and the use of the friction in the lateral direction, the friction compensation algorithm was put forward when vehicle got into large cornering condition to estimate maximum friction coefficient. In Rath *et al*. (2014), a high-order sliding mode observer was developed to estimate the tire friction using the quarter vehicle dynamics model by integrating the nonlinear longitudinal dynamics, the torsional tire dynamics and the nonlinear LuGre friction model. In Sun *et al*. (2015), when vehicle braked emergently, a nonlinear observer was proposed in which the maximum friction coefficient can be estimated by solving an ode through selecting appropriate feedback gain with high computational efficiency.

In this paper, we develop a nonlinear maximum road friction coefficient estimation method making full use of the accurate and controllable torque and angular speed of the in-wheel-motor and Lyapunov stability theory based on tire longitudinal dynamics. The estimation error is proved exponentially stable. First the longitudinal dynamics of each tire is described by modified Burckhardt tire model which includes the maximum friction coefficient explicitly. Then the estimator is designed based on the wheel dynamics to estimate the longitudinal force of the tire and the maximum road friction coefficient. At the meantime, the estimation error of the tire longitudinal force and the maximum road friction coefficient is analysis through Lyapunov stability. The estimation error is proved to converge to zero exponentially if the estimator parameter is chosen appropriate. In order to provide sufficient excitation to the estimator, a slip ratio controller is used here to maintain the slip ratio near the peak of the slip ratio friction coefficient curve. Finally the method is validated with Carsim-Simulink co-simulation and real vehicle tests under multi working conditions in acceleration situation which demonstrates the method is able to estimate the maximum road friction coefficient accurately in real time with high computational efficiency.

This paper is organized as follows. Section 2 presents the tire model. The estimator design and estimation error dynamics are analyzed in Section 3. Estimation strategy is illustrated in Section 4. The experimental setup, validation including simulation and experimental test, procedure, and results are presented and discussed in Section 5. This paper is concluded in Section 6.

2. TIRE MODEL

Burckhardt tire model can describe the relationship between the slip ratio and longitudinal force simply containing maximum road friction coefficient explicitly (Burckhardt, 1993), which means if the longitudinal force and slip ratio are known, the maximum road friction coefficient can be abstracted through mathematical method. In Jin *et al*. (2014), the parameters of the Burckhardt tire model are increased from three to five parameters. The modified Burckhardt tire model is able to describe the real tire longitudinal characteristic more accurately. The modified Burckhardt tire model is shown in Equation (1).

$$\mu(\theta,\lambda)=\theta-\theta e^{-\frac{c_1}{\theta}(\lambda+c_2\lambda^2)}-c_3\lambda\,\mathrm{sgn}(\lambda)+c_4\lambda^2 \tag{1}$$

Here μ is normalized longitudinal tire force and λ is slip ratio.

The parameters in (1) play the following distinctive roles: The peak value of normalized tire force in $\mu-\lambda$ curve is mainly determined by θ which is the maximum road friction coefficient. c_1 dominates the longitudinal slip stiffness at the origin of the $\mu-\lambda$ curve. c_2 can be exploited to adjust the general stiffness of the tire without influencing the stiffness at the origin or the maximum tire force. c_3 and c_4 are positive numbers used to make μ descend a little bit after its peak point. If the two parameters are set to be zero, the $\mu-\lambda$ curve is flat at large slip ratio. Usually $c_2\sim c_4$ vary a little under different road conditions. Based on the experimental test of the tire, the parameters of $c_2\sim c_4$ can be set 8, 0.25, 0.11 respectively.

The influence of θ and c_1 on the shape of the $\mu-\lambda$ curve is shown in Figure 1. The peak value and longitudinal slip stiffness near origin can be adjusted through tuning the values of θ and c_1 respectively.

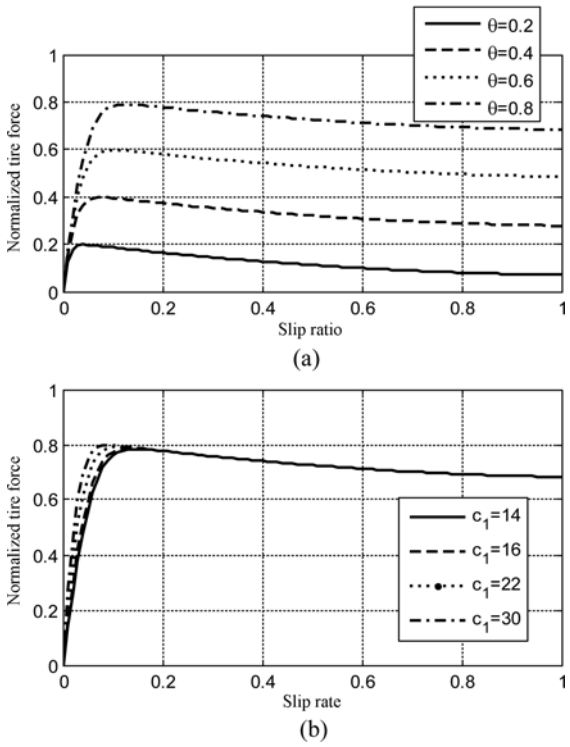

Figure 1. $\mu - \lambda$ curve of modified Burckhardt tire model.

In Figure 1 (a), c_1 is set 18. In Figure 1 (b), θ is set 0.8. As is shown in Figure 1 (b), c_1 has little influence on the peak value of the curve. Therefore, it is reasonable that $c_1 \sim c_4$ are set to constant, which means that the tire model is only determined by the maximum road friction coefficient θ. Based on this innovative assumption, the estimator for θ is proposed.

3. MAXIMUM ROAD FRICTION ESTIMATOR DESIGN

3.1. Wheel Model

The wheel rotational dynamics can be represented as

$$\dot{\omega} = \frac{1}{I_\omega}\left[T_m - \mu(\theta,\lambda)\cdot F_z \cdot r\right] \tag{2}$$

The slip ratio of tire is defined as

$$\lambda = \begin{cases} \dfrac{\omega \cdot r - v_x}{\omega \cdot r}; & v_x < \omega \cdot r \\ \dfrac{v_x - \omega \cdot r}{v_x}; & v_x \geq \omega \cdot r \end{cases} \tag{3}$$

Where ω is wheel angular speed, T_m is the torque delivered to the wheel from the actuator, I_ω is the wheel moment of inertia, r is the tire rolling radius, λ is the slip ratio of the tire, v_x is the longitudinal velocity of the tire, and $\mu(\theta, \lambda)$ is the modified Burckhardt tire model shown in Equation (1). F_z is the wheel normal load calculated by Equation (4) considering the load transfer due to the pitch and roll. *fl*, *fr*, *rl*, *rr* mean front left wheel, front right wheel, rear left wheel, and rear right wheel respectively.

$$\begin{aligned} F_z^{fl} &= mg\frac{l_r}{2l} - m\frac{h_g}{2l}a_x - m\frac{h_g l_r}{B_f l}a_y, \\ F_z^{fr} &= mg\frac{l_r}{2l} - m\frac{h_g}{2l}a_x + m\frac{h_g l_r}{B_f l}a_y, \\ F_z^{rl} &= mg\frac{l_f}{2l} + m\frac{h_g}{2l}a_x - m\frac{h_g l_f}{B_r l}a_y, \\ F_z^{rr} &= mg\frac{l_f}{2l} + m\frac{h_g}{2l}a_x + m\frac{h_g l_f}{B_r l}a_y. \end{aligned} \tag{4}$$

Where m denotes the vehicle mass, g is the gravity acceleration, l_f and l_r are the distances from the front axis and the rear axis to center of gravity (COG), l is the wheel base, h_g is the height of the COG, a_x and a_y are the longitudinal acceleration and lateral acceleration respectively, and B_f and B_r are the front and rear wheel track respectively.

3.2. Estimator Design

The holistic estimator design procedure contains two sections:

(1) The asymptotically stable estimation of θ with the knowledge of the second item in right side of Equation (2).

Last but not least, as the term r/I_ω in Equation (2) is constant, the second item represents the nominal longitudinal tire force $F_x = F_z \cdot \mu(\theta, \omega)$ in this sense. Therefore if the longitudinal tire force is known, we can solve Equation (1) to get the accurate maximum road friction coefficient which means we can transform the estimation of the maximum road friction coefficient into the estimation of the tire longitudinal force η as shown in Equation (5);

$$\eta = -\frac{1}{I_\omega}\cdot\mu(\theta,\lambda)\cdot F_z \cdot r \tag{5}$$

(2) The estimation of the η to guarantee the holistic asymptotically stable estimation of θ and η together.

3.2.1. Estimator design for θ with the knowledge of η

When the longitudinal velocity of the tire is known, λ can be represent by ω through Equation (3). For the convenience of estimator design, the Equation (5) is replaced by

$$\eta = -\frac{r}{I_\omega}\cdot\mu(\theta,\omega)\cdot F_z \tag{6}$$

In this section, for the conciseness of the proof, we assume that $\hat{\eta}$ is equal to η. In next section, we will prove that $\tilde{\theta} = \theta - \hat{\theta}$ and $\tilde{\eta} = \eta - \hat{\eta}$ will converge to zero together where $\hat{\theta}$ is the estimation of θ and $\hat{\eta}$ is the estimation of η. Thus we make that assumption reasonably.

Inspired by Grip *et al*. (2010), based on the lemma E.1 in Krstic *et al*. (1995), we derive the Equation (7) for the

estimation of θ from $\hat{\eta}$.

$$\dot{\hat{\theta}} = \mu_\theta(\omega, \hat{\eta}, \hat{\theta}) = \text{Proj}\left[\gamma \cdot (\theta^*(\omega, \hat{\eta}) - \hat{\theta})\right] \tag{7}$$

Where $\omega \in \Lambda$ is wheel angular speed and bounded, Λ is a compact set, Proj is the projection function and $\theta^*(\omega, \hat{\eta})$ is the unique solution of θ in Equation (6).

Then the dynamics of $\tilde{\theta}$ is given by Equation (8) since we assume θ is constant. The derivative of θ is zero $\dot{\theta} = 0$.

$$\dot{\tilde{\theta}} = \dot{\theta} - \dot{\hat{\theta}} = -\mu_\theta(\omega, \hat{\eta}, \hat{\theta}) = -\mu_\theta(\omega, \hat{\eta}, \theta - \tilde{\theta}) \tag{8}$$

We choose the Lyapunov candidate function as

$$V_u(\tilde{\theta}) = \frac{1}{2}\gamma\tilde{\theta}^2$$

Where γ is a positive constant to be determined.

It is obvious that there exist constant a_1 and a_2 satisfying $0 < a_1 < \frac{1}{2}\gamma$ and $a_2 > \frac{1}{2}\gamma$ respectively such that

$$a_1 \left\|\tilde{\theta}\right\|^2 \le V_u(\tilde{\theta}) \le a_2 \left\|\tilde{\theta}\right\|^2 \tag{9}$$

There exists a_3 subject to $0 < a_3 < \gamma^2$ such that the derivative of the Lyapunov function can be derived and satisfies the following inequality.

$$\begin{aligned} \dot{V}_u(\tilde{\theta}) &= -\frac{dV_u(\tilde{\theta})}{d\tilde{\theta}} \cdot \mu_\theta(\omega, \hat{\eta}, \theta - \tilde{\theta}) \\ &= -\gamma \cdot \tilde{\theta} \cdot \text{Proj}\left[\gamma \cdot (\theta^*(\omega, \hat{\eta}) - \hat{\theta})\right] \end{aligned} \tag{10}$$

$$\dot{V}_u(\tilde{\theta}) \le -\gamma^2 \cdot \tilde{\theta}^2 \le -a_3 \left\|\tilde{\theta}\right\|^2 \tag{11}$$

If $\tilde{\theta} = 0$, then $\theta = \hat{\theta}$, which means

$$\dot{\tilde{\theta}} = -\mu_\theta(\omega, \hat{\eta}, \theta - \tilde{\theta}) = -\text{Proj}\left[\gamma \cdot (\theta^*(\omega, \hat{\eta}) - \hat{\theta})\right] = 0$$

Therefore, $\tilde{\theta} = 0$ is an equilibrium point. According to theorem 4.10 in Khalil (2002), $\hat{\theta}$ will converge to θ ultimately.

In addition, according to the converse theorem of Lyapunov function, there exists a positive constant a_4 such that

$$\left\|\frac{dV_u(\tilde{\theta})}{d\tilde{\theta}}\right\| \le a_4 \left\|\tilde{\theta}\right\| \tag{12}$$

3.2.2. Estimator design for η

The dynamics of the estimation error of η is represented by

$$\dot{\tilde{\eta}} = \dot{\eta} - \dot{\hat{\eta}} \tag{13}$$

According to Equation (6) the dynamics of η is shown by

$$\dot{\eta} = -\frac{1}{I_\omega} \cdot F_z \cdot r \frac{\partial \mu(\theta, \omega)}{\partial \omega} \dot{\omega} \tag{14}$$

The dynamics of $\tilde{\eta}$ is rewriten as

$$\dot{\tilde{\eta}} = -\frac{1}{I_\omega} \cdot F_z \cdot r \frac{\partial \mu(\theta, \omega)}{\partial \omega} \dot{\omega} - \dot{\hat{\eta}} \tag{15}$$

From Equation (7), we obtained

$$\dot{\tilde{\theta}} = -\mu_\theta(\omega, \eta, \hat{\theta}) + \delta(\omega, \tilde{\eta}, \hat{\theta}) \tag{16}$$

Where $\delta(\omega, \tilde{\eta}, \hat{\theta})$ is defined as Equation (17).

$$\delta(\omega, \tilde{\eta}, \hat{\theta}) = \left[\mu_\theta(\omega, \eta, \hat{\theta}) - \mu_\theta(\omega, \hat{\eta}, \hat{\theta})\right] \tag{17}$$

For any compact set Λ, since $\tilde{\theta}$ is bounded, there exists $L_1(\omega) > 0$ for $\delta(\omega, \tilde{\eta}, \hat{\theta})$ satisfying Lipchitz condition in Equation (18).

$$\left\|\delta(\omega, \tilde{\eta}, \hat{\theta})\right\| \le L_1(\omega)\left\|\tilde{\eta}\right\| \tag{18}$$

Then we try to find the suitable form of $\hat{\eta}$ to guarantee that the Equation (19) has the same form as the Equation (16) which is composed by a stable item and a bounded item. If that form of Equation (15) for Equation (19) can be find, according to the theorem 4.18 in Khalil (2002), the estimation error could be bounded at least.

Therefore we assume that $\dot{\tilde{\eta}}$ submit to Equation (19) to backstep for the appropriate form of $\hat{\eta}$.

$$\dot{\tilde{\eta}} = -K \cdot \tilde{\eta} + d(\omega, \tilde{\theta}) \tag{19}$$

Where K is the estimator parameter to be determined.

In addition, we assume $d(\omega, \tilde{\theta})$ submit to Equation (20).

$$\begin{aligned} d(\omega, \tilde{\theta}) &= \frac{1}{I_\omega} \cdot F_z \cdot r \frac{\partial \mu(\hat{\theta}, \omega)}{\partial \omega} \dot{\omega} - \frac{1}{I_\omega} \cdot F_z \cdot r \frac{\partial \mu(\theta, \omega)}{\partial \omega} \dot{\omega} \\ &= -\frac{1}{I_\omega} \cdot F_z \cdot r \cdot \frac{\partial\left(\mu(\theta, \omega) - \mu(\hat{\theta}, \omega)\right)}{\partial \omega} \dot{\omega} \end{aligned} \tag{20}$$

Also for any compact set Λ, since $\tilde{\eta}$ are bounded, there exists $L_2(\omega) > 0$ for $d(\omega, \tilde{\theta})$ satisfying Lipchitz condition in Equation (21).

$$\left\|d(\omega, \tilde{\theta})\right\| \le L_2(\omega)\left\|\tilde{\theta}\right\| \tag{21}$$

In the following, we will prove if there exsists $\hat{\eta}$ such that Equations (19) and (20) hold, then $\tilde{\eta}$ and $\tilde{\theta}$ are asymptotically stable together.

Based on the Equations (16) and (19), for the system composed of $\tilde{\eta}$ and $\tilde{\theta}$, define the new state variable vector $\xi^T = [\tilde{\eta}, \tilde{\theta}]$. Assume the Lyapunov candidate function for the system composed by Equations (16) and (19) is

$$V_c(\xi) = V_u(\tilde{\theta}) + \frac{1}{2}\tilde{\eta}^T\tilde{\eta} \tag{22}$$

Then the derivative of $V_c(\xi)$ can be represented by

$$\begin{aligned} \dot{V}_c(\xi) = &-\frac{dV_u(\tilde{\theta})}{d\tilde{\theta}} \cdot \mu_\theta(\omega, \eta, \hat{\theta}) + \frac{dV_u(\tilde{\theta})}{d\tilde{\theta}} \cdot \delta(\omega, \tilde{\eta}, \hat{\theta}) \\ &- \tilde{\eta}^T \cdot K \cdot \tilde{\eta} + \tilde{\eta}^T \cdot d(\omega, \tilde{\theta}) \end{aligned} \tag{23}$$

From Section 3.2.1 and Equations (18) and (21) we have

$$-\frac{dV_u(\tilde{\theta})}{d\tilde{\theta}}\cdot\mu_\theta(\omega,\eta,\hat{\theta})\le -a_3\left\|\tilde{\theta}\right\|^2 \tag{24}$$

$$\begin{cases}\dfrac{dV_u(\tilde{\theta})}{d\tilde{\theta}}\cdot\delta(\omega,\tilde{\eta},\hat{\theta})\le\left\|\dfrac{dV_u(\tilde{\theta})}{d\tilde{\theta}}\right\|\left\|\delta(\omega,\tilde{\eta},\hat{\theta})\right\| \\ \left\|\dfrac{dV_u(\tilde{\theta})}{d\tilde{\theta}}\right\|\left\|\delta(\omega,\tilde{\eta},\hat{\theta})\right\|\le a_4\cdot L_1(\omega)\left\|\tilde{\theta}\right\|\left\|\tilde{\eta}\right\|\end{cases} \tag{25}$$

$$-\tilde{\eta}^{\mathrm{T}}\cdot K\cdot\tilde{\eta}\le -K\cdot\left\|\tilde{\eta}\right\|^2 \tag{26}$$

$$\tilde{\eta}^{\mathrm{T}}\cdot d(\omega,\tilde{\theta})\le\left\|\tilde{\eta}\right\|\left\|d(\omega,\tilde{\theta})\right\|\le L_2(\omega)\cdot\left\|\tilde{\eta}\right\|\cdot\left\|\tilde{\theta}\right\| \tag{27}$$

Therefore we have

$$\begin{aligned}\dot{V}_c(\xi)\le &-a_3\left\|\tilde{\theta}\right\|^2+a_4\cdot L_1(\omega)\left\|\tilde{\theta}\right\|\left\|\tilde{\eta}\right\| \\ &-K\cdot\left\|\tilde{\eta}\right\|^2+L_2(\omega)\cdot\left\|\tilde{\eta}\right\|\cdot\left\|\tilde{\theta}\right\|\end{aligned} \tag{28}$$

The right side of the inequality can be written as

$$\dot{V}_c(\xi)\le-\zeta^{\mathrm{T}}Q(\omega)\zeta \tag{29}$$

Where

$$Q(\omega)=\begin{bmatrix}K & -\frac{1}{2}\left(L_2(\omega)+a_4\cdot L_1(\omega)\right)\\ -\frac{1}{2}\left(L_2(\omega)+a_4\cdot L_1(\omega)\right) & a_3\end{bmatrix}$$

, and $\zeta^{\mathrm{T}}=\left[\left\|\tilde{\eta}\right\|,\left\|\tilde{\theta}\right\|\right]$.

It is apparent that the first order sequential principal minor of $Q(\omega)$ is positive. Second order sequential principal minor is $a_3\cdot K-\frac{1}{4}\left(L_2(\omega)+a_4\cdot L_1(\omega)\right)^2$.

When $K\ge\frac{(L_2^*+a_4\cdot L_1^*)^2}{4a_3}$, where L_1^* and L_2^* are the upper bound of $L_1(\omega)$ and $L_2(\omega)$ respectively, $\dot{V}_c(\xi)\le-\lambda_{\min}Q(\omega)\zeta^2$ is negative.

Apparently when $\xi^{\mathrm{T}}=0$, $\dot{\xi}=0$ which means $\xi^{\mathrm{T}}=0$ is the equilibrium point. The estimation error ξ^{T} will converge to zero exponentially.

Based on the Equations (6), (14), (19) and (20), we obtain the solution for $\dot{\hat{\eta}}$ as

$$\dot{\hat{\eta}}=-K\left(\frac{1}{I_\omega}T_{\mathrm{m}}+\hat{\eta}\right)+K\dot{\omega}-\frac{1}{I_\omega}\cdot F_z\cdot r\frac{\partial\mu(\hat{\theta},\omega)}{\partial\omega}\dot{\omega} \tag{30}$$

The right side of Equation (30) contains $\dot{\omega}$ which is the derivative of the wheel angular speed. Since wheel angular speed from sensor is largely influenced by the noise, the derivative of the wheel angular speed has poor signal to noise ratio. In order to eliminate the item which contains $\dot{\omega}$, by introducing the new variable y as Equation (31)

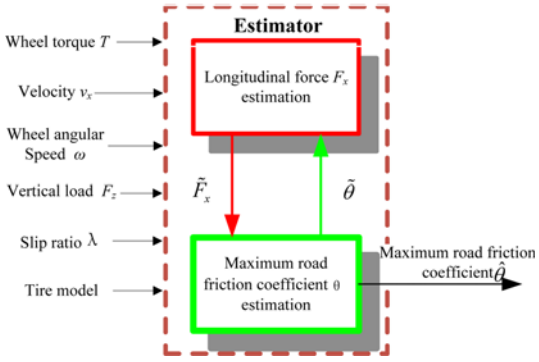

Figure 2. Estimator structure.

shows, we obtain the needed form for $\hat{\eta}$ as Equation (32).

$$\dot{y}=-K\left(\frac{1}{I_\omega}T_{\mathrm{m}}+\hat{\eta}\right)+\frac{1}{I_\omega}\frac{\partial\mu(\hat{\theta},\omega)}{\partial\theta}\cdot F_z\cdot r\cdot\mu_\theta(\omega,\hat{\eta},\hat{\theta}) \tag{31}$$

$$\hat{\eta}=y+K\omega-\frac{1}{I_\omega}F_z\cdot r\cdot\mu(\hat{\theta},\omega) \tag{32}$$

Then the holistic estimator is given by Equations (7), (31) and (32). This estimator contains only two OEDs needed to be solved during the estimation process because there are only two estimated state variables. While if an EKF is used, five ODEs have to be solved simultaneously (Imsland *et al*., 2006). Additionally, in an EKF, the nonlinear model must be linearized at each sample due to the nonlinear tire model, which, along with monitoring of boundedness of the covariance matrix estimate, may involve considerable computation. There is much matrix computation such as the calculation of Kalman gain in the EKF. The matrix computation is great burden to the microprocessor. In this sense, the nonlinear estimator in this paper has great potential when implemented on comercial vehicles.

It is obvious from the nonlinear estimator in Equations (7), (31) and (32) that the estimation results $\hat{\eta}$ of F_x and $\hat{\theta}$ of θ affect each other as shown in Figure 2.

Based on the obove, the estimation error of longitudinal force $\tilde{F}_x$ and maximum road friction coefficient $\tilde{\theta}$ are proved convergence to zero globally and exponentially with appropriate selection of K and γ. Due to the exponential stability of the estimation error, we will set the initial value of $\hat{\theta}$ as 0.8 in simulation and experimental tests to prevent the estimation result starting from zero.

4. ESTIMATION STRATEGY

In the slip ratio controller design, the slip ratio is usually maintained near the optimal slip ratio as far as possible (Van, 2000). As Figure 1 shows, when $c_1 \sim c_4$ are set to fixed constant, the shape of the $\mu-\lambda$ curve is only determined by θ. When slip ratio works near the peak of the curve, sufficient excitation is generated for Equation (12) to solve the equation for $\theta^*(\omega,\hat{\eta})$ algebraically. Therefore in order to improve the estimation accuracy, we

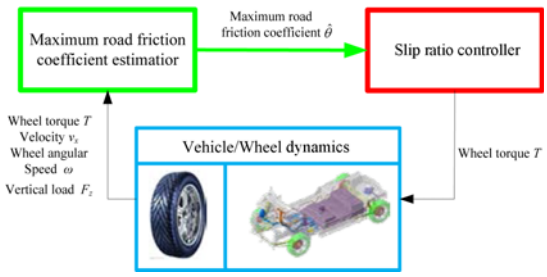

Figure 3. Closed loop estimation system structure.

use a slip ratio controller method according to our previous work in Wang *et al*. (2014) to cooperate with the estimator in the estimation process in simulation and experimental tests. The slip ratio controller is used to control the slip ratio near the optimal slip ratio to ensure enough excitation. The motor torque from slip ratio controller is calculate by Equation (37). The closed loop estimation system structure is shown in Figure 3. On the one hand, the real time estimation result of maximum road friction coefficient updates the parameters in the slip ratio controller, on the other hand, the slip ratio is controlled near the optimal slip ratio. The interaction between each other improves the estimation accuracy.

Based on the estimation of θ, the optimal wheel slip ratio can be derived and according to Equation (3), the optimal wheel slip ratio is equivalent to the optimal wheel anguler speed as shown in Equation (33). Therefore the slip ratio controller is designed to tracking the optimal wheel anguler speed.

$$\omega_{\mathrm{r}} = \frac{v_{\mathrm{x}}}{r(1-\lambda_{\mathrm{r}})} \tag{33}$$

Where λ_{r} is optimal slip ratio and ω_{r} is optimal wheel anguler speed. The tracking error of wheel anguler speed is defined as $e = \omega - \omega_{\mathrm{r}}$. Then combining the wheel dynamics in Equation (2) the dynamics of e is shown as

$$I\dot{e} = \varphi(e) + b(\lambda_{\mathrm{r}}) + T_{\mathrm{m}} \tag{34}$$

Where $\varphi(e)$ and $b(\lambda_{\mathrm{r}})$ are defined as

$$\varphi(e) = r \cdot F_{\mathrm{z}} \left(-\mu(\hat{\theta}, \omega, e) + \mu(\hat{\theta}, \omega_{\mathrm{r}}) \right) \tag{35}$$

$$b(\lambda_{\mathrm{r}}) = -r \cdot F_{\mathrm{z}} \cdot \mu(\hat{\theta}, \omega_{r}) + \overline{T} / 2 \tag{36}$$

Inspired by the contitional intrgrators in Singh and Khalil (2005), we developed this control law in Equation (37) for the wheel slip ratio controller. Details of the proof about the tracking error stability analisis of wheel anguler speed of the slip ratio controller are discussed in the reference (Wang *et al*., 2014).

$$\begin{aligned} \dot{\rho} &= -k_0 \cdot \rho + \alpha \cdot \mathrm{sat}\left(\frac{e + k_0 \rho}{\alpha} \right), |\rho(0)| \le \frac{k_0}{\alpha}, \\ T_{\mathrm{m}} &= -\frac{1}{2}\overline{T} \cdot \mathrm{sat}\left(\frac{e + k_0 \rho}{\alpha} \right) + \frac{1}{2}\overline{T}. \end{aligned} \tag{37}$$

Where $\overline{T}$ is the motor torque upper limit, ρ is the intermediate state variable like y, k_0 and α are positive constants to be designed, ω_{r}' is the reference angular speed, $e = \omega - \omega_{\mathrm{r}}'$ is the angular speed tracking error, and sat is the saturation function.

From the nonlinear estimator in Equations (7), (31) and (32) and the wheel slip ratio controller in Equation (37), we know that the assumption of both the estimator design and slip ratio controller design is that the wheel torque could be accurately known and quickly controllable. Since our test vehicle is the four-in-wheel-motor-drive electric vehicle derived from the commercial vehicle on which we just replaced the driving system and did nothing to the traditional hydraulic braking system, the four motors are the actuators when the vehicle accelerates. However, the traditional hydraulic braking system and the four motors are both actuators when the vehicle brakes. In addition, the hydraulic pressure of the traditional braking system is hard controlled and measured, and the response lag is larger than the motor, which means the wheel torque cannot be accurately known and quickly controlled when the hydraulic braking system intervenes with the motors together. In this sense, in simulation and real vehicle tests, we focus on the acceleration situation with the knowledge of the accurate and controllable wheel torque from the merits of the four-in-wheel-motor-drive electric vehicle.

Fortunately, with the development of the electric hydraulic braking system (EHB) (Xu *et al*., 2015) and the electromagnetic braking system (EMB), it is possible to know and control the wheel torque in the future if the EHB or EMB is implemented on our four-in-wheel-motor-drive electric vehicle, which means the estimation method will be applied in the braking situation in the future work.

5. EXPERIMENT VALIDATION

5.1. Simulation Validation

In simulation procedure, we setup the virtual four-in-wheel-motor-drive electric vehicle in Carsim 8.02 and configure the same parameters of real vehicle to simulate the test vehicle. The parameters of the test vehicle are shown in Tables 1 and 2. Then we established the co-simulation in Matlab/Simulink and CarSim.

From Table 2, we know that front axle is driven by the motor and a gear box with a fixed transmission ratio. The maximum torque to the wheel is sufficient to make tire slip, which means we can use the slip ratio controller to control the slip ratio at the optimal slip ratio to give enough excitation to the estimator for high estimation accuracy. However the motor torque of rear axle is much smaller than front axle such that the tire slip ratio is in the linear region (small slip ratio) in most cases. The slip ratio is too small to generate enough excitation for the estimator leading to the failure of estimating maximum road friction coefficient. Therefore considering the facts of the test vehicle and the characteristic of the estimator, we only

Table 1. Parameters of the test vehicle.

Parameter	Value	Parameter	Value
Mass (kg)	1358	Yaw moment of inertia (kg·m^2)	1835
Wheel base (m)	2.305	Wheel track (mm)	1325 (Front) / 1390 (Rear)
Distance between COG and front axle (m)	1.117	Distance between COG and front axle (m)	1.188
Height of COG (m)	0.525	Tire rolling radius (m)	0.29
Steering ratio	16.68	Front/Rear axle load	54/46

Table 2. Motor parameters of test vehicle.

Parameter	Front axle motor	Rear axle motor
Rated power (kW)	15	5
Peak power (kW)	25	7.5
Rated torque (Nm)	35.8	100
Peak torque (Nm)	90	150
Rated speed (rpm)	4000	480
Maximum speed (rpm)	9500	1350
Gear ratio	6.2	1

choose front axle to validate the effectiveness of the estimator.

In order to simulate the real working condition as far as possible, we add some perturbation and noise in the simulation: we add white noise with 0.1 m/s amplitude and 0.02 s time delay into the longitudinal velocity signal, we add white noise with 0.2 rad/s amplitude and 0.02 s time delay into the wheel angular speed signal and we add 0.005 s time delay into the output of the motor.

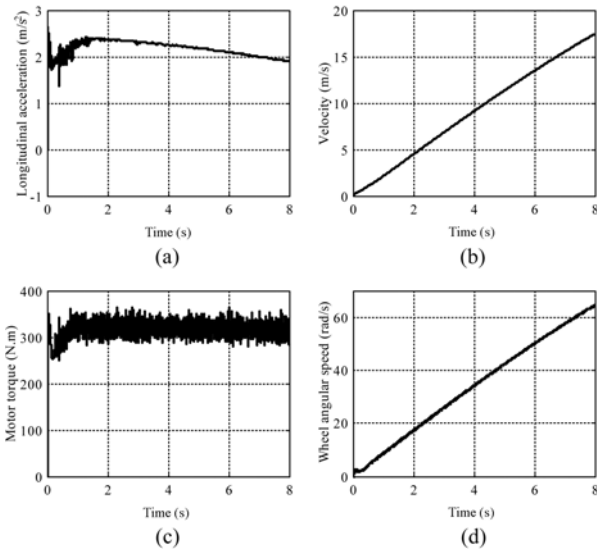

Figure 4. Working condition with full throttle on low maximum road friction coefficient.

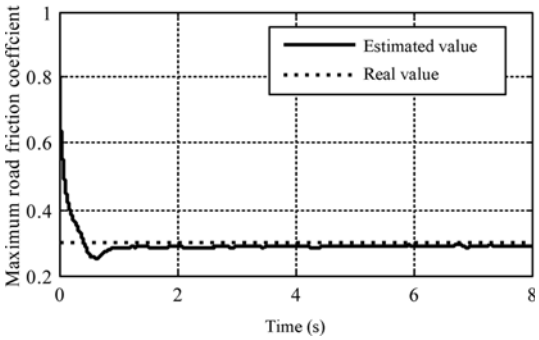

Figure 5. Estimation of maximum road friction coefficient.

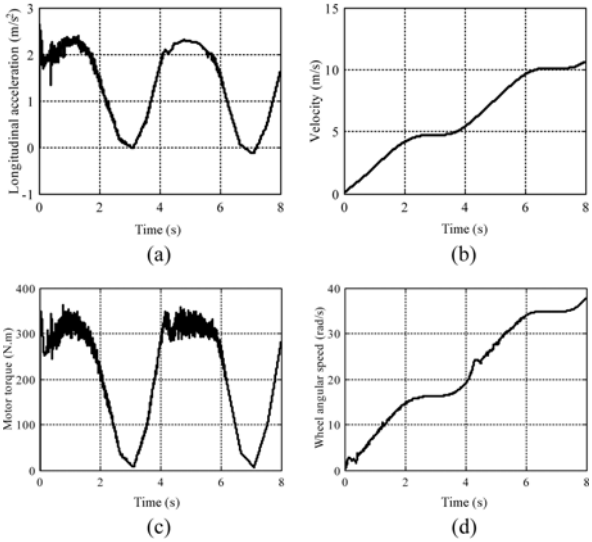

Figure 6. Working condition with sine throttle on low maximum road friction coefficient.

(1) Simulation with low maximum road friction coefficient

a) The vehicle accelerates with full throttle on road where $\theta = 0.3$

b) The vehicle accelerates with sine throttle (amplitude is 0.5, mean value is 0.5, period is 4 s) on road where $\theta = 0.3$

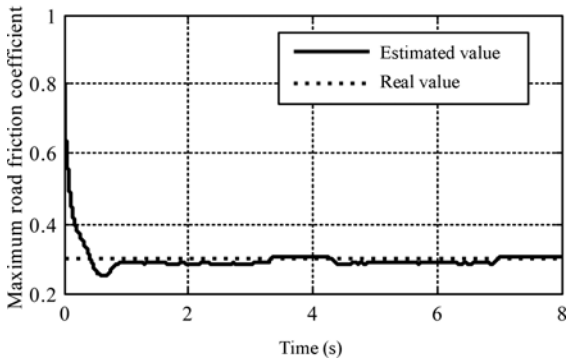

Figure 7. Estimation of maximum road friction coefficient.

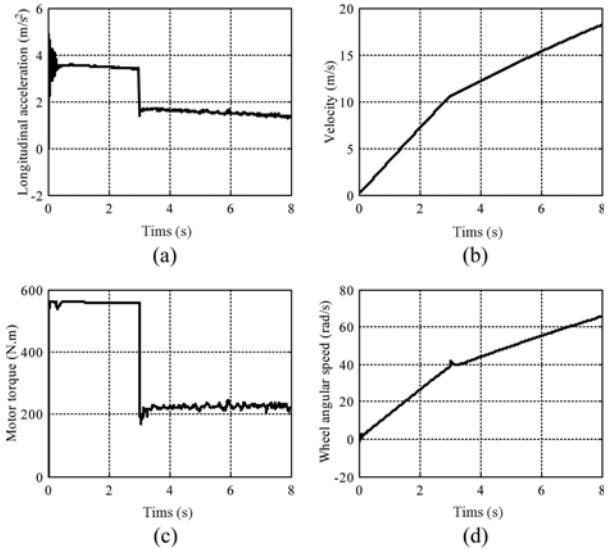

Figure 8. Working condition with full throttle on θ-joint road.

(2) Simulation on high-low maximum road friction coefficient joint road

The vehicle accelerates with full throttle on θ joint road. Before t = 3 s, θ = 0.6. After t = 3 s, θ = 0.2

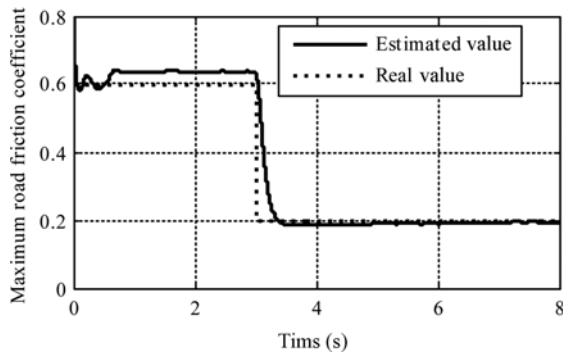

Figure 9. Estimation of maximum road friction coefficient.

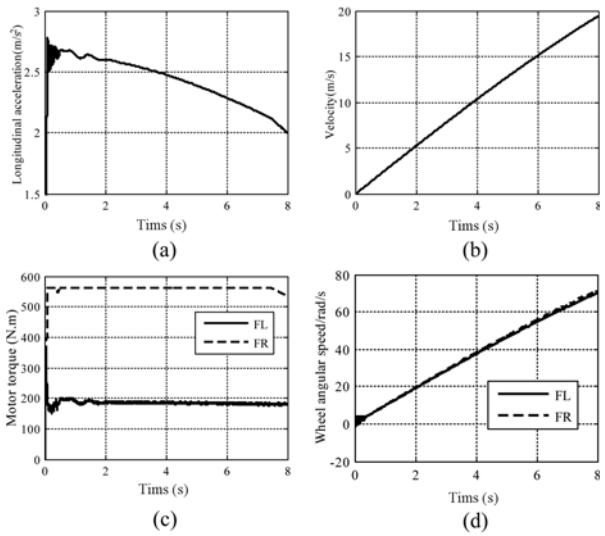

Figure 10. Working condition on θ-split road.

(3) Simulation on maximum road friction coefficient split road

The vehicle accelerates on θ split road. The θ of left road is 0.2 and the θ of right road is 0.6.

Figures 4, 6, 8 and 10 present the four simulation working conditions among which Figures (a) and (b) show the longitudinal acceleration and velocity. Figures (c) and (d) show the motor torque and rotational speed. The first three figures show the working results of the front left wheel and the last shows the working results of the front axle wheels where FL means the front left and FR means the front right.

The estimation results of the maximum road friction coefficient for the front left wheel in first three simulations are shown in Figures 5, 7 and 9. The estimation result of the maximum road friction coefficient for the front axle on θ-split road is shown in Figure 11.

On low θ road with full throttle and sine throttle, the estimator can estimate the real value fast with estimation error less than 0.1 and small overshoot. On high-low θ joint road, the estimator can detect the sudden change of the maximum road friction coefficient within 0.4 s and

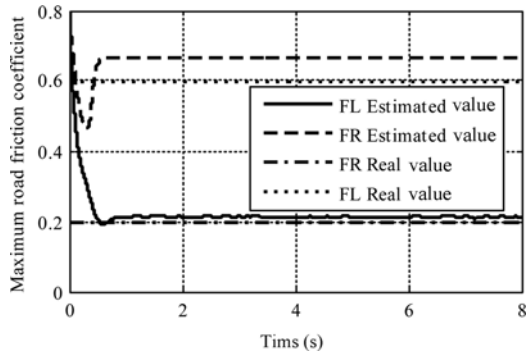

Figure 11. Estimation of maximum road friction coefficient.

estimate the new real value. On the left-right θ-split road, the estimator can distinguish the difference between the left and the right side. The estimation result of each wheel is nearly identical to the real value with estimation error less than 0.1.

5.2. Experimental Validation

The experimental tests were conducted to validate the effectiveness of the proposed method. The test vehicle is setup from a SAIC Roewe E50 driven by four motors among which two hub motors are mounted to the rear axle and two motors and gear boxes are mounted to the front axle. The main parameters of the powertrain are shown in Table 2. Figure 13 shows the test system configuration. A MicroAutoBox from dSPACE is used for real time controller and data acquisition. A GPS-INS RT3003 from Oxford Technical Solutions is used to measure longitudinal velocity and acceleration. The original vehicle gateway can provide the acceleration pedal signal. Motor torque and rotational speed are from motor controller. Based on this measurement system, the maximum road friction estimation method is proposed. The acceleration signal is used to calculate the tire vertical load. The longitudinal velocity and the motor rotational speed are used to calculate the slip ratio of the tire.

The tests were conducted in Maxxis tire proving ground. The tire proving ground contains low maximum road friction coefficient road, high-low maximum road friction coefficient joint road and high-low maximum road friction

Figure 12. Test vehicle.

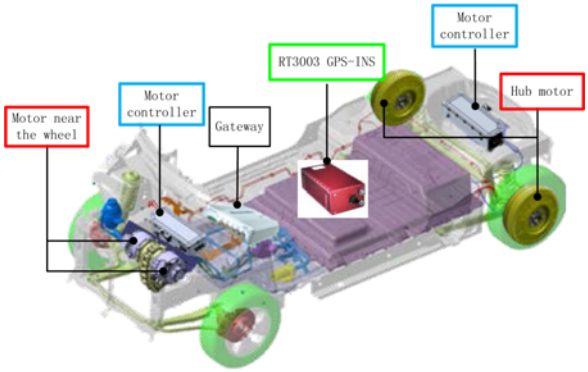

Figure 13. Sensor configuration of test vehicle.

Figure 14. Test on low maximum road friction coefficient road.

coefficient split road. We take the front left tire to analyze in the low θ road and θ joint road and take the two tires of the front axle to analyze for θ-split road condition.

(1) The vehicle accelerates with full throttle on road where $\theta = 0.3$.

The vehicle accelerates on the slippery wet tile road where the maximum road friction coefficient is 0.3. Figure 14 shows the test road.

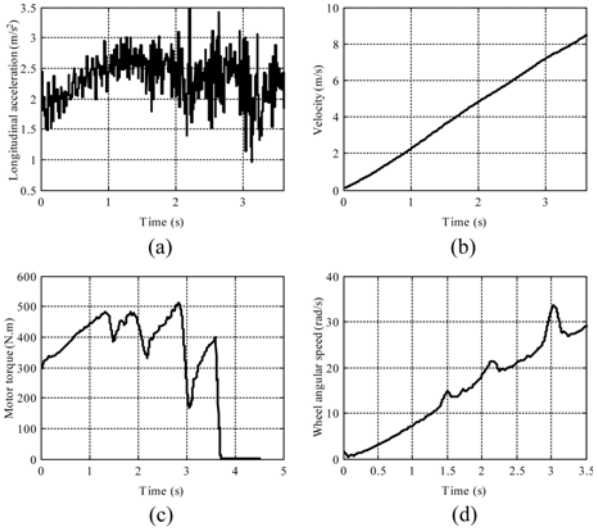

Figure 15. Working condition with full throttle on low maximum road friction coefficient.

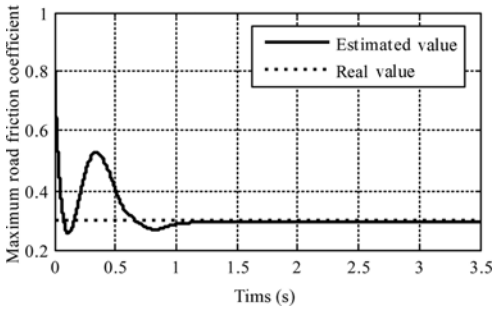

Figure 16. Estimation of maximum road friction coefficient.

Figure 17. Test on high-low maximum road friction coefficient joint road.

(2) The vehicle accelerates on high-low maximum road friction coefficient joint road.
The maximum road friction coefficient before t = 0.32 s is about 0.65. Then vehicle goes into the slippery road where the maximum road friction coefficient is 0.25. Figure 17 shows the test road.

(3) The vehicle accelerates on maximum road friction coefficient split road.
The maximum road friction coefficient of left side is 0.45

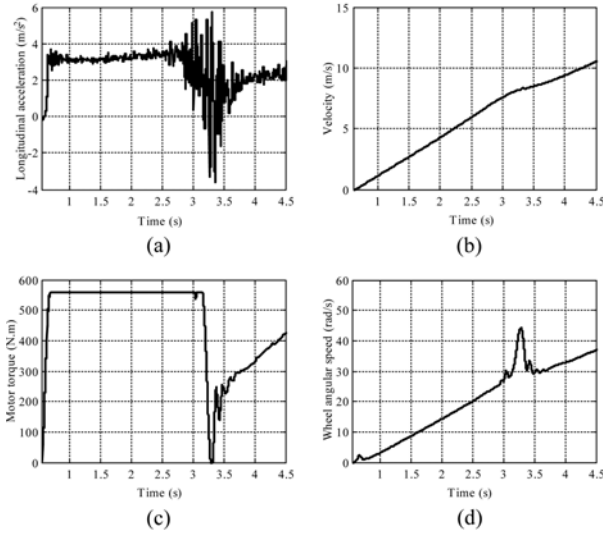

Figure 18. Working condition with full throttle on θ-joint road.

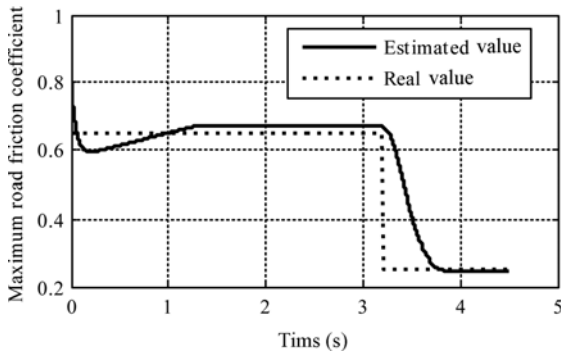

Figure 19. Estimation of maximum road friction coefficient.

Figure 20. Test on θ-split road.

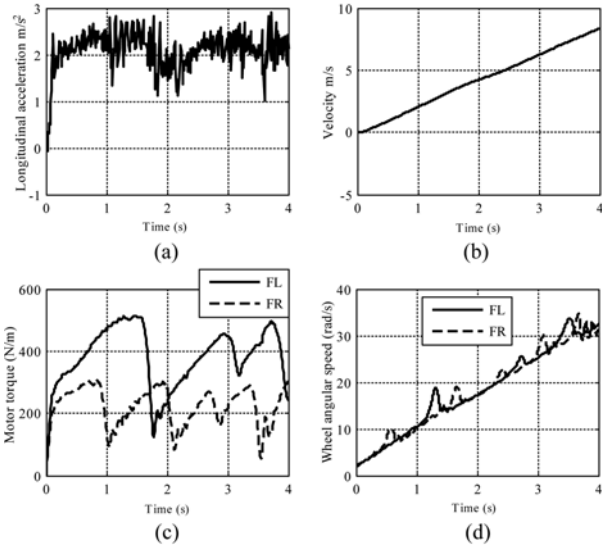

Figure 21. Working condition on θ-split road.

higher than right side where the maximum road friction coefficient is 0.25. Figure 20 shows the test road.

Figures 15, 18 and 21 show the working results of the three test experiments respectively. Figures (a) and (b) show the longitudinal acceleration and velocity. Figures (c) and (d) show the motor torque and rotational speed. The first two figures show the working results of the front left wheel and the last shows the working results of the front axle wheels where FL means the front left and FR means the front right.

The estimation results of the maximum road friction

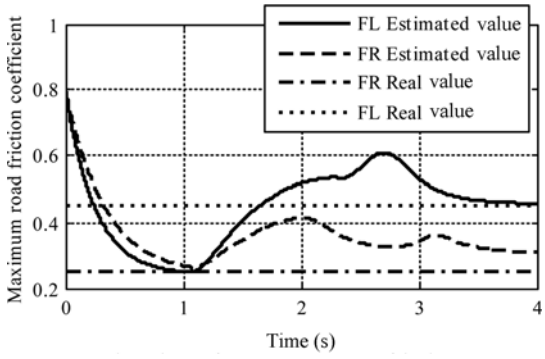

Figure 22. Estimation of maximum road friction coefficient.

coefficient of the front left tire in first two tests are shown in Figures 16 and 19. The estimation result of the maximum road friction coefficient on θ-split road is shown in Figure 22.

When vehicle accelerates on the low friction road, from Figure 16, the estimation result converges to the real value 0.3 quickly from initial value 0.8 in 0.6 s. However, compared with the estimation result of simulation, the overshoot is bigger because the longitudinal velocity and wheel angular speed are very low when the vehicle starts to acceleration, and the signal to noise ratio (SNR) is too low to calculate the accurate slip ratio. On the other hand, the low acceleration will lead to slow increase of the velocity. Therefore the low SNR will last longer than the tests on high-low maximum road friction coefficient joint road. But after t = 0.6 s, the estimation error converges till the end, and a real value 0.3 of the maximum road friction coefficient is acquired. From Figure 19, on the high-low maximum road friction coefficient joint road, at the beginning , the estimation result converges to the real value in 0.3 s, shorter than that on the low friction road. When the vehicle drives into the low friction road, the estimation result quickly converges to 0.26 in 0.4 s. On the θ-split road, the difference of the maximum road friction coefficient between left tire and right tire is 0.2. As Figure 19 shows, the estimator can distinguish the difference between left side and right side. During t = 2 s ~ 3 s, the estimation result fluctuates in an acceptable range. Because the maximum road friction coefficient is different on different side, the longitudinal tire force is also different. The different tire force will generate yaw moment causing the vehicle to yaw. In the meantime there will be lateral force on the tire. However the modified Burckhardt tire model in Section 2 only focuses on the longitudinal characteristic. When there exists lateral force, the tire model cannot describe the tire longitudinal characteristic accurately. That is why the estimation fluctuates. In addition, it will be our future work to research the maximum road friction coefficient estimation under longitudinal and lateral force coupling condition.

In the tests above, although the convergence time is longer than the simulation result, estimation result provides the optimal reference slip ratio for the slip ratio controller to track, which improves the vehicle's driving efficiency. For example, on the θ-split road , during t = 1 s ~ 3 s, the period of fluctuation of estimation result is the same as that of the motor torque and motor rotational speed, as Figure 21 (c) and 22 show. When the tire starts to slip, the accurate maximum road friction coefficient will provide the optimal slip ratio for the slip ratio controller. Therefore the motor torque decreases immediately, the tire returns to the rolling state instead of slipping.

6. CONCLUSION

In this paper, we have demonstrated the development and validation of the maximum road friction coefficient estimation methodology for the four-in-wheel-motor -drive electric vehicle using the real-time precise and controllable motor torque and angular speed. Based on the Lyapunov stability theory, the estimation method is proposed using a modified Burckhardt tire model with five parameters. The estimation error is proved to converge exponentially. This estimation algorithm has high computational efficiency compared with KF theory. On the basis of the simulation and experimental test results, the maximum road friction coefficient could be estimated by the proposed methodology in real-time during longitudinal acceleration on low friction road, high-low friction joint road and high-low friction split road with sufficient excitation provided by the slip ratio controller.

In this study, we assume that no lateral tire force is exerted. The lateral force affects the longitudinal characteristics of the tire. So it needs careful consideration for real vehicle implementation. And the maximum road friction coefficient estimation under longitudinal and lateral force coupling condition will be our future work.

ACKNOWLEDGEMENT–This research is supported by Natianal Natural Science Foundation of China (Grant No. 51475333) and National Basic Research Program of China (Grant No. 2011CB711200).

REFERENCES

Ahn, C., Peng, H. and Tseng, H. E. (2012). Robust estimation of road friction coefficient using lateral and longitudinal vehicle dynamics. *Veh. Syst. Dyn*. **50**, **6**, 961–985.

Ahn, C., Peng, H. and Tseng, H. E. (2013). Robust Estimation of Road Frictional Coefficient. *IEEE Trans. Control Systems Technology* **21**, **1**, 1–13.

Alvarez, L., Yi, J., Horowitz, R. and Olmos, L. (2004). Dynamic friction modelbased tire-road friction estimation and emergency braking control. *J. Dyn. Syst., Meas., Control* **127**, **1**, 22–32.

Burckhardt, M. (1993). Vehicle Chassis Technology-Wheel Sub System. Wurtzburg: Vogel-Verlag.

Chen, L., Bian, M., Luo, Y. and Li, K. (2015). Real-time identification of the tyre–road friction coefficient using an unscented Kalman filter and mean-square-error-weighted fusion. *Proc. IMechE Part D: J. Automobile Engineering*, 1–15.

Chen, Y. and Wang, J. (2011). Adaptive vehicle speed control with input injections for longitudinal motion independent road frictional condition estimation. *IEEE Trans. Vehicular Technology* **60**, **3**, 839–848.

Choi, M., Oh, J. and Choi, S. (2013). Linearized recursive least squares methods for real-time identification of tire – Road friction coefficient. *IEEE Trans. Vehicular Technology* **62**, **7**, 2906–2918.

Erdogan, G., Alexander, L. and Rajamani, R. (2011). Estimation of tire-road friction coefficient using a novel

wireless piezoelectric tire sensor. *IEEE Sensors J.* **11**, **2**, 267–279.

Grip, H. F., Johansen, T. A., Imsland, L. and Kaasa, G. (2010). Parameter estimation and compensation in systems with nonlinearly parameterized perturbations. *Automatica* **46**, **1**, 19–28.

Gustafsson, F. (1997). Slip-based tire-road friction estimation. *Automatica* **33**, **6**, 1087–1099.

Haffner, L., Kozek, M., Shi, J. and Jorgl, H. P. (2008). Estimation of the maximum friction coefficient for a passenger vehicle using the instantaneous cornering stiffness. *American Control Conf.*, Seattle, Washington, USA.

Hori, Y. (2004). Future vehicle driven by electricity and control-research on four-wheel-motored "UOT electric march II". *IEEE Trans. Industrial Electronics* **51**, **5**, 954–962.

Imsland, L., Fossen, T. I., Johansen, T. A., Grip, F. G., Kalkkuhl, J. C. and Suissa, A. (2006). Vehicle velocity estimation using nonlinear observers. *Automatica* **42**, **12**, 2091–2103.

Jin, C., Xiong, L., Yu, Z. and Feng, Y. (2014). Path following control for skid steering vehicles with vehicle speed adaption. *SAE Paper No*. 2014-01-0277.

Khalil, H. K. (2002). *Nonlinear Systems*. Prentice-Hall. Upper Saddle River, New Jersey, USA.

Krstic, M., Kanellakopoulos, I. and Kokotovic, P. V. (1995). *Nonlinear and Adaptive Control Design*. Wiley. New York.

Li, K., Misener, J. A. and Hedrick, K. (2007). On-board road condition monitoring system using slip-based tyre-road friction estimation and wheel speed signal analysis. *Proc. Institution of Mechanical Engineers Part K: J. Multi-body Dynamics* **221**, **1**, 129–146.

Li, L., Jia, G., Song, J. and Ran, X. (2013). Progress on vehicle dynamics stability control system. *Chinese J. Mechanical Engineering* **49**, **24**, 95–107.

Li, L., Wang, F. Y. and Zhou, Q. (2006). Integrated longitudinal and lateral tire/road friction modeling and monitoring for vehicle motion control. *IEEE Trans. Intelligent Transportation Systems* **7**, **1**, 1–19.

Li, L., Yang, K., Jia, G., Song, J. and Han, Z.-Q. (2015). Comprehensive tire-road friction coefficient estimation based on signal fusion method under complex maneuvering operations. *Mechanical Systems and Signal Processing*, **56-57**, 259–276.

Li, L., Zhu, H., Chen, J., Song, J. and Ran, X. (2014). Road Friction identification algorithm for the vehicle stability control. *Chinese J. Mechanical Engineering* **50**, **2**, 132–138.

Lin, F. and Huang, C. (2013). Unscented Kalman filter for road friction coefficient estimation. *J. Harbin Institute of Technology University* **45**, **7**, 115–120.

Matuško, J., Petrović, I. and Perić, N. (2007). Neural network based tire/road friction force estimation. *Engineering Applications of Artificial Intelligence* **21**, **3**, 442–456.

Müller, S., Uchanski, M. and Hedrick, K. (2004). Estimation of the maximum tire-road friction coefficient. *J. Dyn. Syst., Meas., Control* **125**, **4**, 1–11.

Patel, N., Edwards, C. and Spurgeon, S. K. (2008). Tyreroad friction estimation – A comparative study. *Proc. IMechE Part D: J. Automobile Engineering* **222**, **12**, 2337–2351.

Pohl, A., Steindl, R. and Reindl, L. (1999). The intelligent tire utilizing passive SAW sensors measurement of tire friction. *IEEE Trans. Instrumentation and Measurement* **48**, **6**, 1041–1046.

Qi, Z., Taheri, S., Wang, B. and Yu, H. (2015). Estimation of the tyre – Road maximum friction coefficient and slip slope based on a novel tyre model. *Veh. Syst. Dyn.* **53**, **4**, 506–525.

Rajamani, R. (2005). *Vehicle Dynamics and Control*. Springer-Verlag. New York.

Rajamani, R., Piyabongkarn, D., Lew, J. Y., Yi, K. and Phanomchoeng, G. (2010). Tire-road friction-coefficient estimation. *IEEE Control Systems* **30**, **4**, 54–69.

Rath, J. J., Veluvolu, K. C., Defoort, M. and Soh, Y. C. (2014). Higher-order sliding mode observer for estimation of tyre friction in ground vehicles. *IET Control Theory and Applications* **8**, **6**, 399–408.

Ray, L. R. (1997). Nonlinear tire force estimation and road friction identification: Simulation and experiments. *Automatica* **33**, **10**, 1819–1833.

Sato, Y., Kobay, A. D., Kageyama, I., Watanabe, K., Kuriyagawa, Y. and Kuriyagawa, Y. (2007). Study on recognition method for road friction condition. *JSAE Trans*., **38**, 51–56.

Singh, A. and Khalil, H. K. (2005). Regulation of nonlinear systems using conditional integrators. *Int. J. Robust Nonlinear Control* **15**, **8**, 339–362.

Sun, F., Huang, X., Rudolph, J. and Lolenko, K. (2015). Vehicle state estimation for anti-lock control with nonlinear observer. *Control Eng. Practice*, **43**, 69–84.

Van, Z. (2000). Bosch ESP systems: 5 years of experience. *SAE Paper No*. 2000-01-1633.

Wang, X., Xiong, L. and Jin, C. (2014). A control strategy for slip regulation coordinated with driver intention. *Applied Mechanics & Materials*, **556-562**, 4045–4050.

Wit, C. C., Horowitz, R. and Tsiotras, P. (2007). Model-based observers for tire/road contact friction prediction. *Lecture Notes in Control and Information Sciences*, **244**, 23–42.

Xu, S., Yu, Z. and Xiong, L. (2015). Control of novel integrated-electro-hydraulic brake system for automotive. *SAE Paper No*. 2015-01-2699.

Yu, Z., Feng, Y. and Xiong, L. (2013). Review on vehicle dynamics control of distributed drive electric vehicle. *Chinese J. Mechanical Engineering* **49**, **8**, 105–114.

Yu, Z., Zuo, J. and Zhang, L. (2006). A summary on the development status quo of tire-road friction coefficient estimation techniques. *Automotive Engineering* **28**, **6**, 546–549.